PHYSICS AND CHEMISTRY OF SOLID STATE
V. 26, No. 2 (2025) pp. 386-394
Section: Physics

DOI: 10.15330/pcss.26.2.386-394

Vasyl Stefanyk Precarpathian National University

ФІЗИКА І ХІМІЯ ТВЕРДОГО ТІЛА
Т. 26, № 2 (2025) С. 386-394
Фізико-математичні науки

PACS: 81.05.Dz, 61.72.-y

ISSN 1729-4428 (Print)
ISSN 2309-8589 (Online)

A.I. Dobrozhan, G.S. Khrypunov, R.V. Zaitsev, A.V. Meriuts, M.M. Harchenko, A.L. Khrypunova

Crystalline Size and Intrinsic Strain of Hexagonal CdTe Thin Films

National Technical University «Kharkiv Polytechnic Institute», Kharkiv, Ukraine, dobr.abs@gmail.com

In this study, cadmium telluride (CdTe) thin films were synthesized using direct current (DC) magnetron sputtering, and their structural and elastic properties were extensively analyzed. Scanning electron microscopy (SEM) revealed spherical CdTe grains with an average size of approximately 850 nm. X-ray diffraction (XRD) profile analysis, complemented by the Scherrer equation, Scherrer plot, Williamson–Hall (W–H) equations (UDM, USDM, UDEDM), and the Size–Strain Plot (SSP) method, was used to evaluate crystallite size and various elastic properties such as intrinsic strain, microstress, and energy density for different planes respectively. It was observed that crystallite size and intrinsic strain increased with the thickness of the CdTe films, which was attributed to different ionization levels of dissociated Te and Cd atoms at varying sputtering powers.

Keywords: DC magnetron sputtering, elastic properties, CdTe thin film, size–strain plot, X-ray diffraction

Received 02 October 2024; Accepted 14 July 2025.

Introduction

Thin films facilitate the layer-by-layer construction of thin-film semiconductor devices, enabling advantages in economic, dimensional, energy, and other aspects. Thin-film 2D materials exhibit properties distinct from their bulk 3D counterparts, which differ in structural, optical, electrical, and electronic characteristics. The condensation methods further influence the properties of similar materials. In semiconductor thin films, critical optical, electrical, and electronic properties are highly sensitive to thickness constraints [1-4]. Therefore, studying the influence of strain on the properties of thin-film materials is essential. This is especially true for CdTe semiconductor, where lattice strain in a polycrystal can alter the charge carriers' location, excited state lifetimes, absorption properties, and optical band gap. Different methods of material synthesis can significantly impact lattice strain, microstress, and other elastic parameters [5-8], thereby affecting the optical and other semiconductors properties. This material CdTe, with an optical band gap of approximately 1.4 eV, exhibits absorption in the visible and near infrared regions due to quantum confinement, making it highly applicable in solar cells and sensors [9-12].

When employing high-energy direct current magnetron sputtering to produce thin-film layers of cadmium telluride, it is feasible to adjust the sputtering time and magnetron power to achieve layers of varying thicknesses. During the formation of the columnar structure of polycrystalline CdTe at different thicknesses and plasma discharge current densities, crystallites of varying sizes can develop within the material's thickness and plane of the film, impacting its plasticity. Therefore, examining the elastic properties and the effect of doping on these properties is crucial. Among various methods [13-14], the Williamson–Hall (W–H) method is considered one of the most effective and straightforward for studying crystalline size and microstrain properties based on XRD peak analysis. While other methods [13-14] can only determine size and strain, the W–H method allows for determining different elastic properties such as strain and stress energy density from typical X-ray diffraction (XRD) analysis results.

In this study, CdTe thin films were produced using the direct current magnetron sputtering method to investigate their elastic properties. The crystalline nature of these prepared films was characterized by X-ray diffraction (XRD). Further, using different Williamson–Hall (W–H)

equations, such as the uniform deformation model (UDM), uniform stress deformation model (USDM), and the uniform energy density model (UDEDM), various elastic properties such as lattice strain, stress, and energy density were determined for CdTe layers of different thicknesses. Additionally, the lattice strain and size of crystallites were calculated using the Size–Strain Plot (SSP) method to compare with the results obtained from the different (UDM, USDM, and UDEDM) models. Thus, the objective of employing all these models is to examine the impact of magnetron sputtering modes and thickness on the CdTe film's crystalline size and elastic properties.

I. Experimental

To synthesize CdTe thin films using direct current magnetron sputtering (DC magnetron sputtering), a cadmium telluride (CdTe) pressed powder target was initially prepared by cold pressing. The target was subsequently annealed in a vacuum at a temperature range of 60-80°C for 3 hours. A notable feature of the DC magnetron sputtering technology used in this laboratory is the unique design of the magnetron. Specifically, the cooling circuit covered only the magnetic system, eliminating the need for forced cooling of the sputtered target.

Soda-lime glass substrates were installed in a substrate holder equipped with a mobile heater. To facilitate the thermionic emission of electrons from the target material and ignite the plasma discharge, the target underwent preheating for 15 minutes. Following this, a "target training" process was conducted for 5 minutes. After completing the "training" process, the substrate holder, carrying the substrate, was moved into position above the target without altering the discharge electrical parameters or the pressure within the chamber. The distance from the substrate to the target was maintained at 40 mm.

The deposition process was carried out under controlled conditions to achieve different thicknesses of CdTe films. The thickness of the films was adjusted by varying the sputtering time and the magnetron power. During the formation of the columnar structure of polycrystalline CdTe, crystallites of different sizes were formed within the material's thickness and plane, depending on the plasma discharge current density. These variations in crystallite size significantly influenced the material's plasticity and other mechanical properties.

The morphology of uncoated CdTe samples was observed using scanning electron microscopy (SEM) in the secondary electron mode. The SEM instrument used was a "Tescan Vega 3LMH", operating at an accelerating voltage of 30 kV without additional conductive coatings.

The structure of the obtained CdTe thin films was studied by X-ray diffractometry (XRD) methods. Automatic recording of X-ray spectra was conducted using *Θ-2Θ* scanning on an X-ray diffractometer type DRON, with a step size of 0.01-0.02 degrees, utilizing Kα-radiation of a Co anode (λ = 0.1788996 nm).

II. Results and discussion

2.1. SEM Analysis of CdTe thin film surface

SEM image for surface CdTe thin film is shown in Figure 1. Average crystal sizes on thin film surfaces have been obtained at approximately 850 and 900 nm for different samples.

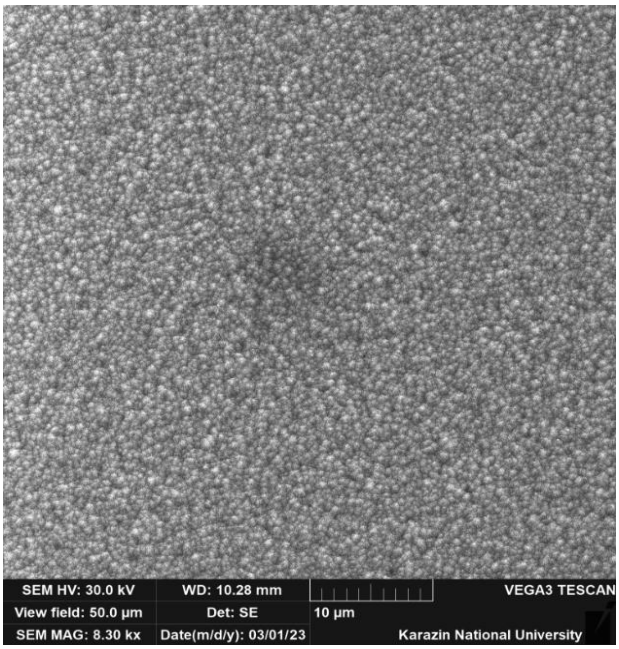

Fig. 1. SEM image of surface CdTe thin film - sample 3.

2.2. X-ray Diffraction (XRD) Analysis

In Fig. 2, the X-ray diffraction (XRD) patterns of magnetron-sputtered CdTe thin films are depicted. All patterns confirm the hexagonal structure of the obtained samples when compared with data from the JCPDS software. Specifically, XRD peaks are observed at 27.5, 49.5, 79.8, and 91.0 degrees, corresponding to the (002), (103), (105), and (006) planes of CdTe, respectively. Moreover, the intensity of these XRD peaks decreases as the angle (2θ) increases, particularly for higher-order planes. This gradual decrease in intensity with higher Miller indices (hkl) is a typical pattern observed in the XRD spectra of CdTe. Typically, there is a dominant peak with the highest intensity in most XRD patterns due to the prevalence of such planes within the material—in this case, the (002) plane. The intensity of other peaks also follows a decreasing trend with higher Miller indices and increasing 2θ values, indicating the presence of fewer such planes in the material.

The instrumental corrected broadening (β) of the diffraction peak is expressed in terms of broadening due to instrument (βi) as [15],

$$\beta = [\beta_0^2 - \beta_i^2]^{\frac{1}{2}} \quad (1)$$

where β_0 is the experimentally observed broadening. The average crystallite size has been determined using the corrected full width at half maximum (FWHM) for each peak, applying Scherrer's equation [16],

$$D = \frac{k\lambda}{\beta \cos \Theta} \quad (2)$$

where β is the corrected FWHM of each XRD peak in radians, and Θ is the diffraction angle. In this equation, Scherrer's constant k is taken as 1, and the X-ray wavelength λ is 0.1788996 nm. The average crystallite size was calculated to range from 30 to 49 nm. Additionally, the lattice constants a, c, and d-spacing were also computed from the XRD data using Eq. 3, with the results presented in Table 1. [17],

$$\lambda = 2d \sin \Theta \quad (3)$$

As evident from Table 1, the calculated lattice constant values for different planes show only slight variations. The close agreement of the lattice constant value for the (002) plane with previously reported values for hexagonal CdTe, along with the alignment of all peak positions with the reported positions, confirms that the calculated lattice constant values for the other planes, as presented in Table 1, are accurate and reliable.

The average size also has been obtained graphically using Scherrer plot as shown in Fig. 3 (1-4), which is drawn with $1/\beta$ along X-axis against $cos\Theta$ along Y-axis as per the modified Scherrer equation, given in Eq 4 [18],

$$\cos \Theta = \frac{k\lambda}{D}\left(\frac{1}{\beta}\right) \quad (4)$$

From the slope of the extrapolated linear fitted plot, the crystalline sizes for CdTe thin films have been obtained from 30 nm to 48 nm. Further, these XRD data have been analyzed to study the effect of magnetron sputtering modes on the elastic properties of CdTe thin films by modified Williamson–Hall equation.

2.2.1 Determination of Size and Strain Using Williamson–Hall Method

Ideally, X-ray diffraction peaks exhibit a delta function for bulk materials. However, for thin films, these peaks undergo broadening owing to the crystallite size effect and intrinsic lattice strain effect. Consequently, through peak broadening analysis, it becomes feasible to derive values for intrinsic strain and average crystallite size, along with other elastic properties, utilizing modified Williamson-Hall equations such as the Uniform Deformation Model (UDM) equation, Uniform Strain Deformation Model (USDM) equation, and Uniform Deformation and Elastic Distortion Model (UDEDM) equation.

According to Williamson–Hall method, the total broadening in a XRD peak is given by [19],

$$\beta_{hkl} = \beta_D + \beta_\varepsilon \quad (5)$$

where β_{hkl} is the total broadening, β_D corresponds to broadening due to size and β_ε corresponds to the broadening due to strain. Again, as per Stokes–Wilson equation, the intrinsic strain is expressed as [20],

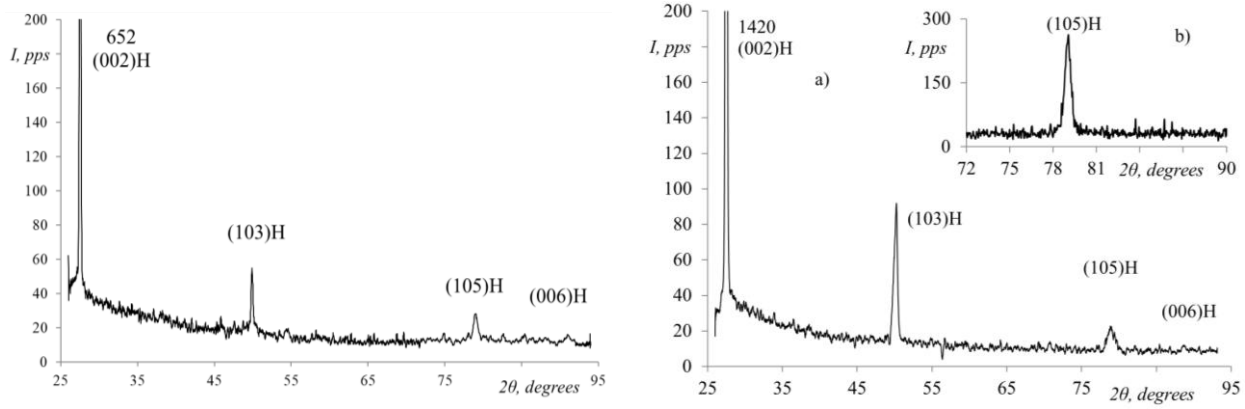

Fig. 2. X-ray diffraction patterns of CdTe thin films: Sample 1 (left) and Sample 3 (right, a, b).

Table 1.

Calculated values of lattice constant a, c and d-spacing for different (hkl) plane CdTe thin films

№	I, mA	2Θ, grad	(hkl) planes	d, nm	a, nm	c, nm	<D>, nm	$<\varepsilon> *10^{-3}$, a.u.
1	40	27.52	(002)	0.376	0.459	0.752	39.52	3.07
		49.89	(103)	0.212				
		78.98	(105)	0.141				
		91.07	(006)	0.125				
2	60	27.49	(002)	3.764	0.459	0.752	48.02	3.78
		91.03	(006)	1.254				
3	80	27.48	(002)	3.770	0.454	0.753	30.24	4.34
		50.14	(103)	2.110				
		78.89	(105)	1.410				
		91.01	(006)	1.254				
4	80	27.50	(002)	3.763	0.456	0.753	38.95	3.69
		78.97	(105)	1.407				
		90.99	(006)	1.254				

$$\varepsilon = \frac{\beta_s}{4tg\Theta} \quad (6)$$

Therefore, (5) can be written after rearrangement as,

$$\beta_{hkl}\cos\Theta = \frac{k\lambda}{D} + 4\varepsilon\sin\Theta \quad (7)$$

This equation is the UDM equation. A graph is then plotted with the term $4sin\Theta$ along X-axis and $\beta_{hkl}cos\Theta$ along Y-axis for different (hkl) planes both all samples of CdTe thin films, which are shown in the Fig. 4 (1-4), respectively. Here, the intercept and slope of the graph gives the crystallite size and the lattice strain, respectively, which are given in Table 2.

Now, if the strain value is small in thin films, which consist of nanocrystals, then according to the USDM model, uniform stress can be considered in all crystallographic directions. For uniform stress and small strain value, Hook suggested a generalized law between the strain and stresses, which is given as, $\sigma=\varepsilon\bullet Yhkl$, where σ is the uniform stress in the crystal and Y_{hkl} denotes the modulus of elasticity. Thus, using Hook's law in Eq 7 the modified Williamson–Hall equation for USDM is as follows [21],

$$\beta_{hkl}\cos\Theta = \frac{k\lambda}{D} + \frac{4\sigma\sin\Theta}{Y_{hkl}} \quad (8)$$

Now, the values of Y_{hkl} can be calculated from the following formula as per hexagonal structure of the samples [22],

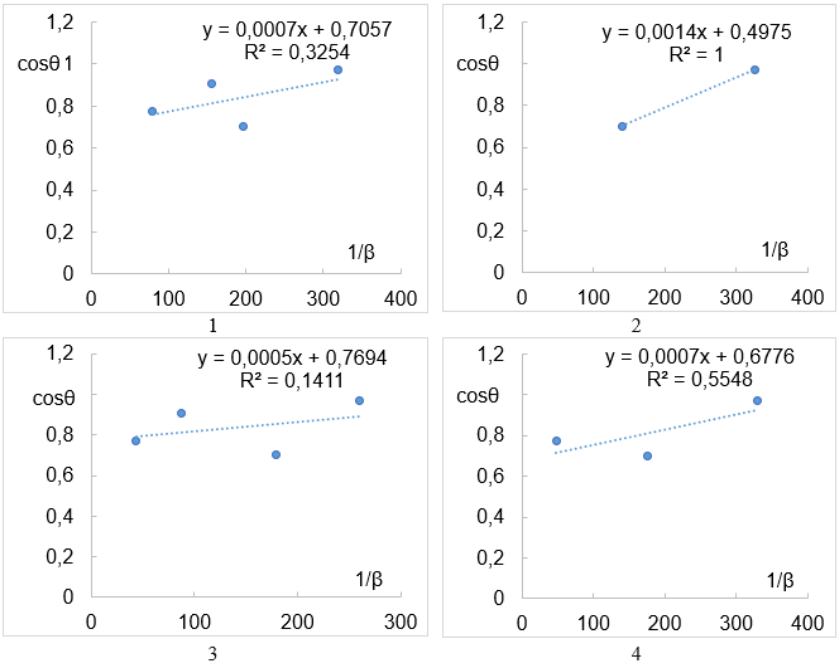

Fig. 3. Scherrer plots for all samples of CdTe thin films.

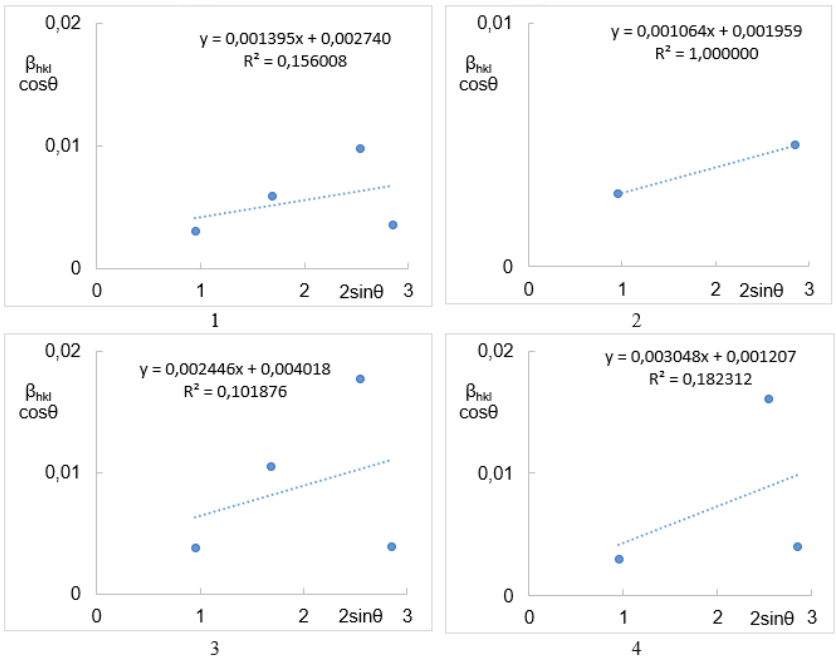

Fig. 4. Uniform deformation model (UDM) graph for all samples of CdTe thin films.

Table 2.

Stiffness constant value of hexagonal cadmium telluride (CdTe)

Cadmium telluride (CdTe) HEX					
C_{11}, GPa	C_{12}, GPa	C_{13}, GPa	C_{33}, GPa	C_{44}, GPa	C_{66}, GPa
62.2	35.9	29.1	68.9	13.1	13.15

$$\frac{1}{Y_{hkl}} = \frac{\left[h^2+\frac{(h+2k)^2}{3}+\left(\frac{a}{c}l\right)^2\right]^2}{\left[s_{11}\left(h^2+\frac{(h+2k)^2}{3}\right)^2+s_{33}\left(\frac{a}{c}l\right)^4+(s_{44}+2s_{13})\left(h^2+\frac{(h+2k)^2}{3}\right)\left(\frac{a}{c}l\right)^2\right]} \quad (9)$$

In this Eq 9, S_{11}, S_{13}, S_{33} and S_{44} denote the elastic compliances of the hexagonal CdTe and (hkl) are the miller indices. Again, the relation between the elastic compliances (S_{11}, S_{13}, S_{33} and S_{44}) are as follows [23]. Values of the elastic compliances S_{11}, S_{13}, S_{33} and S_{44} have been found as 0.019011, 0.005409, 0.019366 and 0.076336 GPa-1, respectively.

Using these elastic compliances values in Eq 9, Y_{hkl} values have been calculated for the respective (hkl) planes, which are given in Table 3.

Table 3.

Value of modulus of elasticity in different (*hkl*) XRD plane

Sample	Different XRD planes	Value of Y_{hkl}
CdTe HEX	(002)	51.64
	(103)	40.56
	(105)	45.00
	(006)	51.64

Thereafter, plotting the term $\beta_{hkl}Cos\Theta$ along Y-axis with $4Sin\Theta/Y_{hkl}$ along X-axis, the graph of USDM for all samples CdTe thin films are shown in Fig. 5 (1-4) respectively. The intercept and the slope of the plots give the values of size and stress which are given in Table 4.

A real crystal is imperfect due to the presence of various defects and dislocations. As a result, the linear relationship between stress and strain, assumed by the USDM model, does not apply to real crystals. Therefore, the uniform deformation energy density model (UDEDM) is needed, as it accounts for uniform anisotropic lattice strain across all crystallographic orientations. According to Hooke's law, the energy density and strain are related by the following equation, $U=\varepsilon^2\times(Y_{hkl}^2)$ where U is the energy density and the relation between energy density and stress is given by $U=\sigma^2/Y_{hkl}$. Therefore, according to UDEDM model, the Eq 8 can be re-written in terms of energy density as [21],

$$\beta_{hkl}\cos\Theta = \frac{k\lambda}{D} + 4\sin\Theta\left(\frac{2U}{Y_{hkl}}\right)^{\frac{1}{2}} \quad (10)$$

Graphs are plotted with $\beta_{hkl}Cos\Theta$ in X-axis and $4Sin\Theta$ $(2/Y_{hkl})^{0,5}$ in Y-axis as shown in Fig.6 (1-4). The crystallite size and energy density were determined from the slope

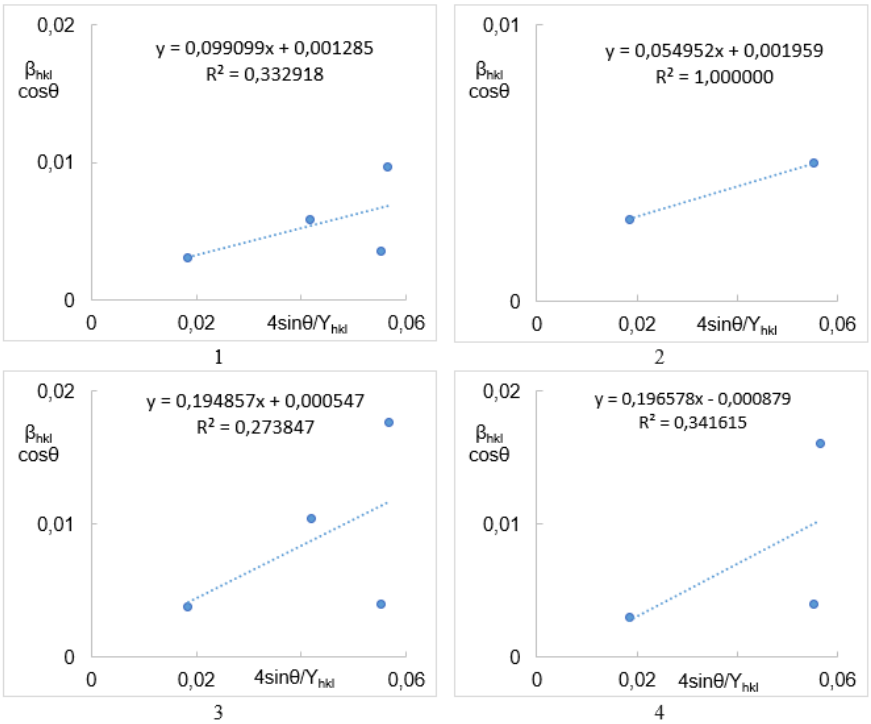

Fig. 5. Uniform stress deformation model (USDM) graph for all samples of CdTe thin films.

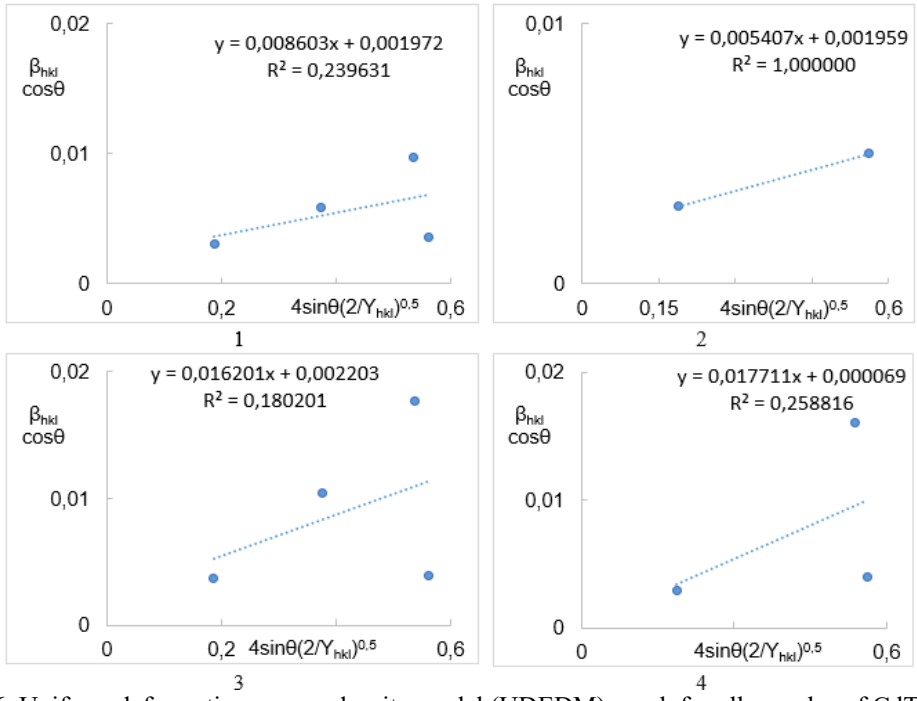

Fig. 6. Uniform deformation energy density model (UDEDM) graph for all samples of CdTe thin films.

Table 4.

Crystalline size and strain calculation using UDM and USDM model for all samples of CdTe thin films

	Size, nm		UDM model		USDM model		
Sample	Scherrer equation	Scherrer plot	Size, nm	Strain * 10^{-3}, a.u.	Size, nm	Stress, Gpa	Strain * 10^{-3}, a.u.
1	39.52	254.54	65.30	1.40	139.22	0.10	2.10
2	48.02	123.46	91.32	1.11	91.32	0.05	1.06
3	30.24	374.27	44.52	2.45	327.06	0.19	4.13
4	38.95	240.88	148.22	3.05	203.53	0.20	3.98

Table 5.

Crystalline size and strain calculation using UDEDM model and SSP method for all samples of CdTe thin films

	UDEDM model				SSP method	
Sample	Size, nm	Energy Density, KJ/m^3	Stress, GPa	Strain * 10^{-3}, a.u.	Size, nm	Strain * 10^{-3}, a.u.
1	90.72	740.12	0.06	1.77	71.78	1.01
2	91.32	292.36	0.04	1.06	71.56	0.56
3	81.21	2624.72	0.11	3.34	27.95	1.30
4	259.27	3136.80	0.12	3.56	30.09	0.99

and intercept of the graphs, with the corresponding values presented in Table 5. It was observed that the slope in each graph for the respective model is positive. This positive slope indicates an increase in lattice spacing [24], which results in a larger lattice constant due to the accumulation of sliding structural defects within the grain boundaries of the polycrystalline material. The increase in the lattice constant value has already been confirmed through Equation 4, where the average lattice constant c for CdTe is listed in Table 1. The relationship between increasing lattice spacing and the positive slope can be attributed to the XRD peak widths. As the value of 2Θ changes, the intensity and peak width of the X-ray pattern decrease, depending on the crystallographic planes. This can also be observed in the decrease in the interplanar distance a, as shown in Table 1.

2.2.2 Size–Strain Plot (SSP) Method

The Size–Strain Plot (SSP) method for XRD peak profile analysis models the peak as a combination of Lorentzian and Gaussian functions, where size broadening is represented by the Lorentzian function and strain broadening by the Gaussian function. In contrast, the Williamson–Hall (W–H) method considers peak broadening as a function of the X-ray diffraction angle 2Θ [25]. In the SSP method, total peak broadening is the sum of both Lorentzian and Gaussian contributions. Taking this into account, the relationship between crystallite size and strain is described by the following equation in the SSP method [25],

$$(d_{hkl}\beta_{hkl}\cos\Theta)^2 = \frac{k\lambda}{D}(d_{hkl}^2\beta_{hkl}\cos\Theta) \qquad (11)$$

decreasing strain with thickness of samples. This variation

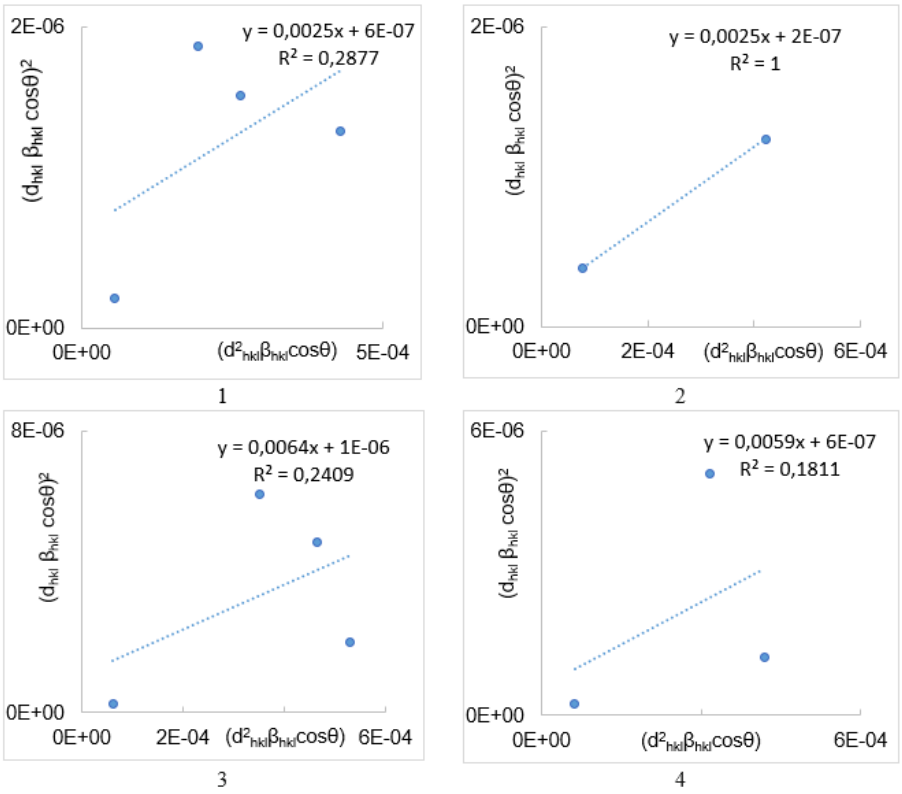

Fig. 7. Size strain plot (SSP) graph for all samples of CdTe thin films.

In this equation, d_{hkl} is the separation of two (hkl) planes. The SSP plots are shown in Fig.7 (1-4), where the graph is plotted with the term $(d_{hkl}\beta_{hkl}cos\Theta)^2$ along Y-axis against the term $d_{hkl}{}^2\beta_{hkl}cos\Theta$ along X-axis as per Eq 11. The size and strain for all samples are given in Table 5.

From the data in each sample and the corresponding table, it was observed that the CdTe crystalline size varies with different powers of magnetron sputtering. This variation is attributed to the differential ionization of dissociated Te and Cd atoms at varying sputtering powers. This reduction in the average size of the ionic radii can increase the values of elastic properties, particularly the intrinsic strain.

Table 4 presents the estimated size and deformation values derived from UDM and USDM. Although the values slightly differ across models, all models indicate an increase in crystallite size and internal strain with higher magnetron power and deposition rates. Table 4 also suggests that similar parameter increases are associated with greater thickness of CdTe films and the accumulation of sliding defects within the film. As the crystallite size decreases, the strain value increases due to slight alterations in atomic arrangements caused by size constraints, leading to lattice narrowing or broadening, and consequently, higher lattice strain and stress values [26]. The percentage increase in intrinsic strain is significantly higher in the USDM model since it accounts for anisotropic strain along different lattice plane directions, while the UDM model results from isotropic modeling.

Moreover, both the UDEDM and SSP models, as shown in Table 5, reveal a reduction in crystallite size with occurs because UDEDM accounts for uniform anisotropic strain across different lattice planes, linked to the strain energy density resulting from defects and dislocations in the crystal structure. Additionally, UDEDM provides voltage and energy density values that increase with the thickness of the CdTe films. While all models rely on XRD peak broadening analysis, the SSP model uniquely combines Lorentzian (size broadening) and Gaussian (strain broadening) functions for peak profile analysis. As a result, the SSP model produces average size values that closely align with those obtained from SEM analysis (as shown in Tables 4 and 5). Nonetheless, the other models also offer comparable results, correlating crystallite size and strain values with various elastic properties.

Conclusions

In this work, CdTe thin-film layers were synthesized by DC magnetron sputtering. SEM images show that the CdTe grains on the surface of the films with an average size of about 850 nm, respectively. In addition to XRD profile analysis, the CdTe crystallite size was evaluated using the Scherrer equation, Scherrer plot, W–H equation considering UDM, USDM and UDEDM and SSP method along with various elastic properties such as strain, stress and energy density. It was observed that the size of the crystallites increases with the increase in the thickness of the CdTe films and also increases the elastic properties, especially the inherent deformation.

The study observed that increasing the film thickness enhances the elastic properties, particularly the intrinsic strain. This was confirmed by all models, indicating a

consistent trend of increasing crystallite size and internal strain with higher magnetron power and deposition rates. The intrinsic strain values were higher in the USDM model, which considers anisotropic strain along different lattice plane directions. The UDEDM model also highlighted the significance of strain energy density due to defects and dislocations.

Acknowledgments

The work was carried out with the financial support of the National Research Fund of Ukraine, project for the implementation of scientific research and development 2022.01/0014, "Development of an experimental sample of a film element for the protection of electronic equipment against pulses of electromagnetic radiation."

Dobrozhan A.I. – associate professor of the micro- and nanoelectronic department;
Khrypunov G.S. – professor, vice-rector for scientific and pedagogical activity;
Zaitsev R.V. – professor, head of the micro- and nanoelectronic department;
Meriutz A.V. – associate professor of the micro- and nanoelectronic department;
Harchenko M.M. – researcher of the micro- and nanoelectronic department;
Khrypunova A.L. – associate professor of the micro- and nanoelectronic department.

[1] N. Romeo, A. Bosio, R. Tedeschi, A. Romeo, V. Canevari, *A highly efficient and stable CdTe/CdS thin film solar cell,* Solar Energy Materials and Solar Cells, 58(2), 209 (1999); https://doi.org/10.1016/S0927-0248(98)00204-9.
[2] M.V. Kirichenko, R.V. Zaitsev, A.I. Dobrozhan, G.S. Khrypunov, M.M. Kharchenko, 2017 IEEE 1st Ukraine Conference on Electrical and Computer Engineering, UKRCON (Kyiv, 2017), p. 355 (2017); https://doi.org/10.1109/UKRCON.2017.8100509.
[3] G.S. Khrypunov, G.I. Kopach, A.I. Dobrozhan, R.P. Mygushchenko, O.V. Kropachek, V.M. Lyubov, *Structure and optical properties of CdS polycrystalline layers for solar cells based on CdS/CdTe*, Functional Materials, 26 (1), 23 (2019); https://doi.org/10.15407/FM26.01.23.
[4] A. Dobrozhan, A. Meriuts, G. Kopach, R. Mygushchenko, *Structure and Optical Properties of Thermal CdTe Thin Films after Electron Beam Irradiation* 2021 IEEE 2nd KhPI Week on Advanced Technology, KhPI Week (Kharkiv, 2021), 701 (2021); https://doi.org/10.1109/KhPIWeek53812.2021.9570022.
[5] A. Dobdozhan, A. Meriuts, A. Khrypunova, 2023 IEEE 4th KhPI Week on Advanced Technology, KhPI Week (Kharkiv, 2023) https://doi.org/10.1109/KhPIWeek61412.2023.10312950.
[6] P.C. Dey, R. Das, *Impact of silver doping on the crystalline size and intrinsic strain of MPA-capped CdTe nanocrystals: a study by williamson–Hall method and size–strain plot method,* J. of Materi Eng and Perform 30, 652 (2021); https://doi.org/10.1007/s11665-020-05358-9.
[7] P.C. Dey, R. Das, *Effect of silver doping on the elastic properties of CdS nanoparticles,* J. Indian J. Phys., 92, 1099 (2018); https://doi.org/10.1007/s12648-018-1214-4.
[8] Y. Ren, X. Gao, C. Zhang, X. Liu, S. Sun, *The Electronic and Elastic Properties of Si Atom Doping in TiN: A First-Principles Calculation,* Coating, 8(1) 4(2018); https://doi.org/10.3390/coatings8010004.
[9] G.I. Kopach, R.P. Mygushchenko, G.S. Khrypunov, A.I. Dobrozhan, M.M. Harchenko, *Structure and Optical Properties CdS and CdTe Films on Flexible Substrate Obtained by DC Magnetron Sputtering for Solar Cells,* Journal of Nano- and Electronic Physics, 9(5), 05035 (2017); https://doi.org/10.21272/jnep.9(5).05035.
[10] A.I. Dobrozhan, G.I. Kopach, R.P. Mygushchenko, G.S. Khrypunov, M.M. Harchenko, O.V. Polezhaeva, 2018 IEEE 8th International Conference on Nanomaterials: Applications and Properties, (Odesa, 2018) art. no. 8915293 (2018); https://doi.org/10.1109/NAP.2018.8915293.
[11] D. Kudii, A. Meriuts, A. Khrypunova, T. Shelest, V. Varvianska, R. Zaitsev, 2020 IEEE 4th International Conference on Intelligent Energy and Power Systems, (Istanbul, 2020) art. no. 9263233, 135 (2020): https://doi.org/10.1109/IEPS51250.2020.9263233.
[12] R.V. Zaitsev, M.V. Kirichenko, G.S. Khrypunov, S.A. Radoguz, M.G. Khrypunov, D.S. Prokopenko, L.V. Zaitseva, *Operating Temperature Effect on the Thin Film Solar Cell Efficiency,* Journal of Nano- and Electronic Physics, 11(4), 04029 (2019); https://doi.org/10.21272/jnep.11(4).04029.
[13] B.P. Pandey, *Structural and Elastic Properties Calculation of CdX (X= S, Se, Te) Semiconductors from First-Principles,* International Journal of Applied Nanotechnology, 3(2), 8 (2017); https://doi.org/10.37628/ijan.v3i2.303.
[14] S. Mahadevan, S.P. Behera, G. Gnanaprakash, T. Jayakumar, J. Philip, B.P.C. Rao, *Size distribution of magnetic iron oxide nanoparticles using Warren–Averbach XRD analysis,* J. Phys. Chem. Solids, 73, 867 (2012); https://doi.org/10.1016/j.jpcs.2012.02.017.
[15] S. Sarkar, R. Das, *Determination of structural elements of synthesized silver nano-hexagon from X-ray diffraction analysis,* Indian J. Pure Appl. Phys., 56(10), 765 (2018); https://doi.org/10.56042/ijpap.v56i10.19809.
[16] R. Das, S.S. Nath, R. Bhattacharjee, *Preparation of linoleic acid capped gold nanoparticles and their spectra.* Physica E Low Dimens. Syst. Nanostruct., 43(1), 224 (2010); https://doi.org/10.1016/j.physe.2010.07.008.
[17] N. Kurniawati, D.A.P. Wardani, B. Hariyanto, N.P. Har, N. Darmawan, Irzaman. *Analysis of Lattice Constants and Error for The Hexagonal Crystal Structure of Silicon Dioxide Using The Cramer-Cohen Method,* J. Phys.: Conf. Ser. 2019 012071 (2021); https://doi.org/10.1088/1742-6596/2019/1/012071.

[18] R. Jacob, J. Isac, *X-ray diffraction line profile analysis of $Ba_{0.6}Sr_{0.4}Fe_xTi_{(1-x)}O_{3-\delta}$', (x=0.4),* Int. J. Chem. Stud., 2(5), 12(2015).
P. Bindu, S. Thomas, *Estimation of lattice strain in ZnO nanoparticles: X-ray peak profile analysis,* J. Theor. Appl. Phys., 8, 123 (2014); https://doi.org/10.1007/s40094-014-0141-9.
[20] M.S.S. Saravanan, K. Sivaprasad, P. Susila, S.P. Kumaresh, Physica B, 406(2), 165 (2011); https://doi.org/10.1016/j.physb.2010.10.023.
[21] R. Das, S. Sarkar, *X-ray diffraction analysis of synthesized silver nanohexagon for the study of their mechanical properties,* Mater. Chem. Phys., 167, 97 (2015); https://doi.org/10.1016/j.matchemphys.2015.10.015.
[22] J.-M. Zhang, Y. Zhang, K.-W. Xu, V. Ji, *Anisotropic elasticity in hexagonal crystals*, Thin Solid Films 515, 7020 (2007); https://doi.org/10.1016/j.tsf.2007.01.045.
[23] S. Saib, S. Benyettou, N. Bouarissa, S. Ferahtia, *First principles study of structural, elastic and piezoelectric properties of $CdSe_xTe_{1-x}$ ternary alloys in the wurtzite structure*, Phys. Scr., 90, 035702 (2015); https://doi.org/10.1088/0031-8949/90/3/035702.
[24] P.V. Raleaooa, A. Roodt, G.G. Mhlongo, D.E. Motaung, O.M. Ntwaeaborwa, *Analysis of the structure, particle morphology and photoluminescent properties of $ZnS:Mn^{2+}$ nanoparticulate phosphors,* Optik, 153, 31 (2018); https://doi.org/10.1016/j.ijleo.2017.09.120.
[25] A.K. Zak, W.H. Abd Majid, M.E. Abrishami, R. Yousefi, *X-ray analysis of ZnO nanoparticles by Williamson-Hall and size-strain plot methods,* Solid State Sci., 13, 251 (2011); https://doi.org/10.1016/j.solidstatesciences.2010.11.024.
[26] D. Nath, F. Singh, R. Das, *Calculating the Crystallite Size of Microsorum scolopendria AgCl Nanoparticles and Their Biological Activities*, Mater. Chem. Phys., 239, 122021 (2020); https://doi.org/10.1016/j.matchemphys.2019.122021.

А.І. Доброжан, Г.С. Хрипунов, Р.В. Зайцев, А.В. Меріуц, М.М. Харченко, А.Л. Хрипунова

Розмір кристалітів та внутрішні напруження гексагональних тонких плівок CdTe

Національний технічний університет «Харківський політехнічний інститут», м. Харків, Україна, dobr.abs@gmail.com

У цьому дослідженні тонкі плівки телуриду кадмію (CdTe) були отримані за допомогою магнетронного розпилення на постійному струмі, і їх структурні та пружні властивості були детально проаналізовані. Скануюча електронна мікроскопія (SEM) виявила сферичні зерна CdTe із середнім розміром приблизно 850 нм. Аналіз профілю рентгенівської дифракції (XRD), доповнений рівнянням Шеррера, графіком Шеррера, рівняннями Вільямсона–Холла (W–H) (UDM, USDM, UDEDM) і методом графіку розміру-деформацій (SSP), використовувався для визначення оцінки розміру кристалітів і різних пружних властивостей, такі як деформація, напруга та щільність енергії. Було помічено, що розмір кристалітів і власна деформація збільшувалися зі збільшенням товщини плівок CdTe, що пояснювалося різними рівнями іонізації дисоційованих атомів Te і Cd при різних потужностях магнетронного розпилення.

Ключові слова: магнетронне розпилення на постійному струмі, пружні властивості, тонка плівка CdTe, графік розміру-деформації, рентгенівська дифракція